2352 Vol. 34, No. 11 / November 2017 / Journal of the Optical Society of America B Research Article

Journal of the Optical Society of America B OPTICAL PHYSICS

Intensity correlation in frequency upconversion via four-wave mixing in rubidium vapor

Yong Sup Ihn,[1] Kwang-Kyoon Park,[1] Yosep Kim,[1] Young-Tak Chough,[2] and Yoon-Ho Kim[1,*]

[1]Department of Physics, Pohang University of Science and Technology (POSTECH), Pohang 37673, South Korea
[2]Department of IT-Automotive Engineering, Gwangju University, Gwangju 61743, South Korea
*Corresponding author: yoonho72@gmail.com

Received 19 July 2017; accepted 19 September 2017; posted 21 September 2017 (Doc. ID 302863); published 16 October 2017

We report a study on the transfer of intensity correlation properties in frequency upconversion via four-wave mixing (FWM) in rubidium (Rb) vapor. The $5S_{1/2}-5P_{3/2}-5D_{5/2}$ two-photon transition in ^{85}Rb leads to collimated blue light (CBL) generation at 420 nm by absorbing two input photons of wavelengths 780 nm and 776 nm. The $g^{(2)}(\tau)$ intensity correlation measurement of the CBL field reveals that the intensity correlations of the input fields are transferred to the CBL field due to strong atomic coherence in the FWM loop. We also demonstrate that the measured values of $g^{(2)}(\tau)$ of the CBL field are reduced by the effect of Doppler broadening of Rb vapor.

OCIS codes: (190.7220) Upconversion; (270.1670) Coherent optical effects; (190.4975) Parametric processes; (190.4380) Nonlinear optics, four-wave mixing.

https://doi.org/10.1364/JOSAB.34.002352

1. INTRODUCTION

Atomic coherence induced by resonant atom-photon interaction can give rise to efficient nonlinear frequency mixing processes. One such example is frequency upconversion or collimated blue light (CBL) generation via four-wave mixing (FWM) in alkali atomic vapor [1–4]. Experiments on CBL typically has been focused on the efficiency of CBL generation [5–7]. CBL at 420 nm on the order of a few tens of microwatts to milliwatts has been achieved by applying an additional coupling laser to a hyperfine ground state [5] or by optimizing the input laser polarization and frequencies [6]. Saturation of CBL has also been observed [7]. More recently, CBL has been investigated for orbital angular momentum transfer in the diamond-type FWM scheme [8]. Such a process, for instance, may be used to identify the nonlinear processes formed via different FWM loops [9,10]. To date, however, transfer of intensity correlation properties of input fields in the CBL process involving the diamond-type FWM scheme has not been reported, although it has been shown that atomic electromagnetically induced transparency (EIT) medium preserves the intensity correlation property during the EIT storage and retrieval [11–14]. In this work, we experimentally demonstrate the intensity correlation transfer in the CBL generation in ^{85}Rb atomic vapor as a result of the parametric FWM process. It is shown that the second-order intensity correlation function, $g^{(2)}(\tau)$, measured for the 420 nm CBL beam follows the intensity correlations of the 780 nm and 776 nm input beams. We also investigate the reduction of the $g^{(2)}(\tau)$ of the CBL beam due to the Doppler broadening effect of rubidium (Rb) vapor through numerical simulation.

2. EXPERIMENTAL SETUP

The schematic of the experimental setup and the relevant Rb energy levels are shown in Fig. 1. We first briefly describe the CBL generation process in the ^{85}Rb energy level diagram. The two input fields at 780 nm and 776 nm drive the coherent atomic transition from $5S_{1/2}$ to $5D_{5/2}$, resulting in 5.23 μm amplified spontaneous emission to $6P_{3/2}$. Large atomic population at $6P_{3/2}$ then leads to CBL generation at 420 nm [15].

In the experiment, two independent external cavity diode lasers are used for generating 780 nm and 776 nm beams, which are on resonant to $5S_{1/2} \rightarrow 5P_{3/2}$ and $5P_{3/2} \rightarrow 5D_{5/2}$ transitions of ^{85}Rb, respectively. To frequency-lock the two lasers for the $5S_{1/2}-5P_{3/2}-5D_{5/2}$ two-photon resonance, small portions of the two lasers are picked off by beam splitters and the counterpropagating beams are overlapped in a Rb vapor cell heated at 40°C. The 780 nm laser is kept locked to the saturated-absorption peak for the $5S_{1/2}(F=3)$ to $5P_{3/2}(F'=4)$ transition, and the frequency of the 776 nm laser is adjusted to maximize the frequency upconversion efficiency. The orthogonally polarized 780 nm and 776 nm input beams are first combined by a polarizing beam splitter (PBS), as shown in Fig. 1. The combined beam is turned into circular polarization with a quarter-wave plate (QWP) and then focused

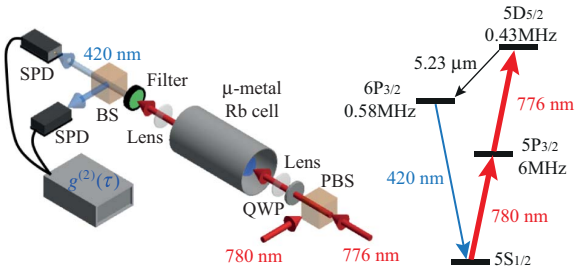

Fig. 1. Experimental setup and ^{85}Rb atomic energy levels. PBS, polarizing beam splitter; QWP, quarter-wave plate; filter, 420 nm bandpass filter; BS, beam splitter; SPD, single-photon detector.

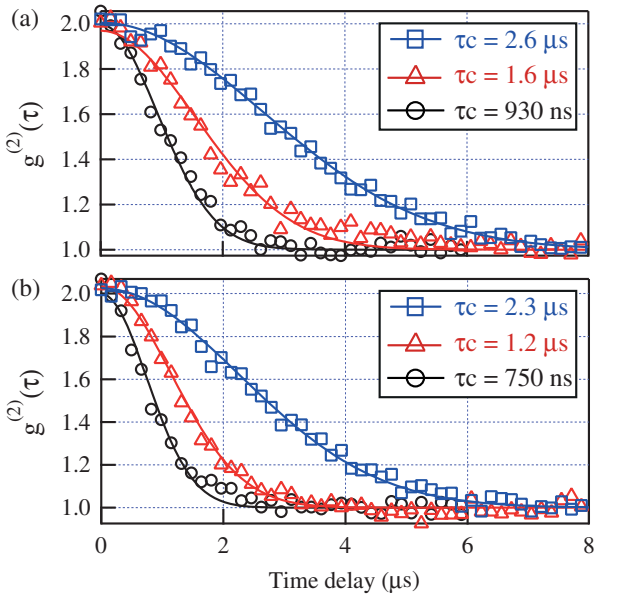

Fig. 2. Second-order correlation function, $g^{(2)}(\tau)$, measured for (a) the 780 nm thermal input beam and (b) the 776 nm thermal input beam. Depending on the speed of the rotating ground disk, we are able to vary the coherence time τ_c. The width of the time bin for the data points is 20 ns. The solid lines represent fitting results according to Eq. (2).

into the Rb vapor cell. The Rb vapor cell was surrounded with three layers of μ-metal sheets to prevent Earth's magnetic field and was kept at room temperature. The second-order correlation function $g^{(2)}(\tau)$ of the 420 nm CBL beam, generated as a result of the FWM process, is measured with the Hanbury-Brown–Twiss (HBT) interferometer consisting of a beam splitter (BS), two single-photon detectors (SPDs) (Perkin-Elmer SPCM-AQRH-13), and a time-correlated single-photon counting system (Picoharp 300) [16]. To be able to demonstrate transfer of intensity correlations from the input beams to the CBL beam, we use different photon statistics combinations for the input 780 nm and 776 nm beams. As the laser beam exhibits the Poisson photon statistics that are uncorrelated in the intensity fluctuation, we also prepare intensity-correlated input beams with the Bose–Einstein photon statistics by using the rotating ground disk method for generating pseudothermal light [17]. In experiment, we measure $g^{(2)}(\tau)$ of the 420 nm CBL beam to observe how it depends on the combinations of intensity correlations of the input beams.

3. EXPERIMENTAL RESULTS

For chaotic light or thermal light, the second-order correlation function $g^{(2)}(\tau)$ can be written as [18,19,20]

$$g^{(2)}(\tau) = \frac{\langle I(t)I(t+\tau)\rangle}{\langle I(t)\rangle^2} = 1 + |g^{(1)}(\tau)|^2, \quad (1)$$

where $g^{(1)}(\tau)$ is the first-order correlation function, which is the Fourier transform of the power spectrum. It is well known that, for thermal light, $g^{(2)}(0) = 2$, which suggests strong photon bunching, while $g^{(2)}(\tau) = 1$ for coherent light such as laser. Figure 2 shows measured $g^{(2)}(\tau)$ for the pseudothermal input beams before entering the Rb cell. The single count rates of SPDs were around 6 kHz, with the background noise count rate of around 300 Hz. In Fig. 2, we use the following function:

$$g^{(2)}(\tau) = 1 + \exp(-\tau^2/2\tau_c^2) \quad (2)$$

for fitting the data considering the random nature used for the pseudothermal light generation method. Here τ is the electronic time delay, and τ_c is the coherence time. The coherence times depend on the angular speed of the rotating ground disk used for generating the thermal light [11,21].

We now look at how the intensity correlation of CBL beam is affected by the combinations of the 780 nm and 776 nm input beams with Poisson and Bose–Einstein photon statistics. The experimental data, $g^{(2)}(\tau)$, measured for the CBL beam with different combinations of the 780 nm and 776 nm input beams, are shown in Fig. 3. First, the data in Fig. 3(a) show the $g^{(2)}(\tau)$ measured for the 420 nm CBL beam generated by the coherent (intensity uncorrelated) 776 nm input beam and the pseudothermal (intensity correlated) 780 nm input beam with the three different τ_c shown in Fig. 2(a). Now, in Fig. 3(b), we show the $g^{(2)}(\tau)$ measured for the 420 nm CBL beam generated by the coherent 780 nm input beam and the pseudothermal 776 nm input beam with the three different τ_c shown in Fig. 2(b). In both Figs. 3(a) and 3(b), the coherence times of the 420 nm CBL beam closely follow those of the 780 nm or 776 nm thermal input beam, and this is a good indication that the intensity correlation of the input beam is transferred to the CBL beam.

Figure 3(c) shows the $g^{(2)}(\tau)$ measured for the 420 nm CBL beam when both 776 nm and 780 nm beams have intensity correlations with the coherence times shown in Fig. 2. It is interesting to note that the peak values of the second-order correlation function, $g^{(2)}(0)$, are higher in this case (both input beams are thermal) than those in Fig. 3(a) and in Fig. 3(b) (i.e., only one of the inputs is thermal). We attribute this result to the fact that both input fields contribute to CBL generation due to two-photon coherence via the parametric FWM process. Finally, we look at the $g^{(2)}(\tau)$ measured for the 420 nm CBL beam when both 776 nm and 780 nm beams are coherent; see Fig. 3(d). As expected, the result clearly indicates that the intensity fluctuation of the CBL beam is uncorrelated in this case.

4. THEORETICAL ANALYSIS

Although the experimental data in Fig. 3 clearly demonstrate that the intensity correlation of the input beam is transferred to

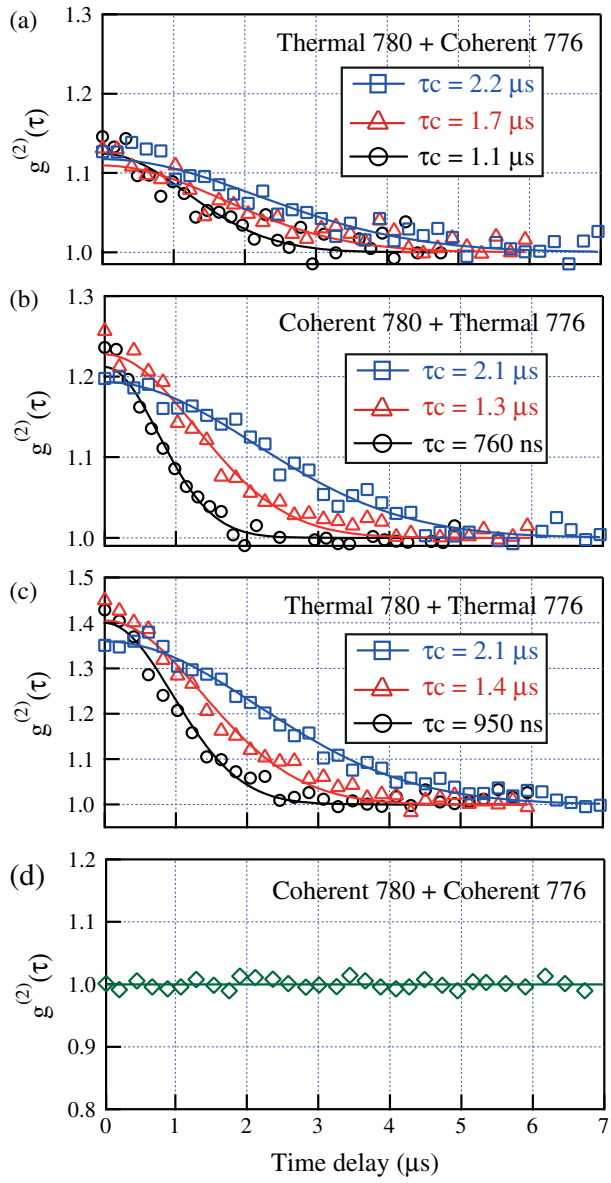

Fig. 3. $g^{(2)}(\tau)$ measured for the CBL beam with different combinations of the 780 nm and 776 nm input beams with intensity correlated or uncorrelated. (a) Coherent 776 nm input and pseudothermal 780 nm input with the three different τ_c shown in Fig. 2(a). (b) Coherent 780 nm input and pseudothermal 776 nm input with the three different τ_c shown in Fig. 2(b). (c) Both 780 nm and 776 nm beams are pseudothermal. (d) Both 780 nm and 776 nm beams are coherent. The width of the time bin for the data points is 40 ns. The solid lines represent fitting results according to Eq. (2).

the CBL beam via the parametric FWM process, we, however, notice that the peak values of $g^{(2)}(\tau)$ for the CBL beams, $g^{(2)}(0)$, are much smaller than those of the input beams, which are all saturated at the theoretical maximum of $g^{(2)}(0) = 2$. Even though the background noise contribution is taken into account in the reduction of $g^{(2)}(\tau)$, in the case of cold atoms, there is no significant reduction of $g^{(2)}(\tau)$ value [22]. Therefore, we reckon that the reduced $g^{(2)}(0)$ for the CBL beam is the result of Doppler broadening of the Rb vapor. In order to identify the effect of Doppler broadening to the CBL $g^{(2)}(0)$ values, we carried out another experiment, shown in Fig. 4. Here, we measure the $g^{(2)}(\tau)$ function of spontaneous emission of Rb vapor due to the 780 input beam with different photon statistics (correlated and uncorrelated intensity fluctuation). To avoid the input beam's intensity correlation inadvertently affecting that of the Rb spontaneous emission, the $g^{(2)}(\tau)$ of the Rb spontaneous emission is measured at the side of the Rb vapor cell, as shown in the experimental setup. In this experiment, a 780 nm laser was first frequency-locked to the $5S_{1/2}(F = 3) - 5P_{3/2}(F' = 4)$ transition. The 780 nm input beam (coherent or pseudothermal) was then sent to a ^{85}Rb vapor cell. The μ-metal shielding of the Rb cell was removed to collect the spontaneous emission from the side of the Rb cell. Then, by using the HBT setup shown in Fig. 4, the $g^{(2)}(\tau)$ of the spontaneous emission was measured.

The experimental data are shown in Fig. 4. In Figs. 4(a) and 4(c), we show the $g^{(2)}(\tau)$ measurement of the coherent and pseudothermal input 780 nm beam, respectively. For the coherent 780 nm input, the $g^{(2)}(\tau)$ measurement of the spontaneous emission is shown in Fig. 4(b). Interestingly, it has the coherence time τ_c of 580 ps, which is much shorter than the excited-state lifetime of 26 ns, which clearly is due to Doppler broadening in the Rb vapor cell. The $g^{(2)}(\tau)$ was measured with 0.1 ns-wide time bins, the single count rates of the detectors were approximately 6 kHz, and the total data accumulation time was 15 h. The reduction of the peak value $g^{(2)}(0)$ is due to the fact that the measurement time-bin window of 100 ps is comparable to the 500 ps timing resolution of the electronics [19–20]. For the pseudothermal 780 nm input, the $g^{(2)}(\tau)$ measurement of the spontaneous emission is shown in Fig. 4(d). We notice that, while the input pseudothermal 780 nm beam has the peak value of $g^{(2)}(0) = 2$, the Rb spontaneous emission has significantly reduced peak value $g^{(2)}(0) \approx 1.25$, similar to Fig. 4(b). This result may be explained as both the Doppler broadening and the pseudothermal input affecting the observed $g^{(2)}(\tau)$ value.

We now consider theoretically the reduction of $g^{(2)}(0)$ due to the contribution of Doppler broadening. We start from the fact that the second-order correlation function for thermal light is given by $g^{(2)}(\tau) = 1 + |g^{(1)}(\tau)|^2$. Here, $g^{(1)}(\tau)$ is the Fourier transform of the power spectrum of the thermal light. The light spectrum emitted from an atomic vapor cell can be obtained by calculating the convolution between the spectral profile of the incident laser, the atomic cross section, and the Maxwell–Boltzmann distribution of the atomic velocities depending on the temperature T [22]:

$$S(\omega) \propto \iiint \mathrm{d}\omega' \mathrm{d}v_x \mathrm{d}v_y S_0(\omega') \sigma\left[\omega'\left(1 - \frac{v_x}{c}\right)\right] \times e^{-\frac{v_x^2 + v_y^2}{u^2}} \delta\left[\omega - \omega'\left(1 - \frac{v_x}{c}\right)\left(1 + \frac{v_y}{c}\right)\right]. \quad (3)$$

The above equation considers an atom absorbing a photon of frequency $\omega'(1 - \frac{v_x}{c})$, which then emits a photon along the y direction with frequency $\omega'(1 - \frac{v_x}{c})(1 + \frac{v_y}{c})$ in the laboratory frame. The power spectrum of the incident laser is $S_0(\omega') = e^{-\frac{(\omega' - \omega_0)^2}{2(\Delta\omega)^2}}$, where $\Delta\omega = 2\pi \times 0.5$ MHz and $\omega_0 = \frac{2\pi c}{\lambda_0}$ with $\lambda_0 = 780$ nm. The Lorentzian cross section is given by

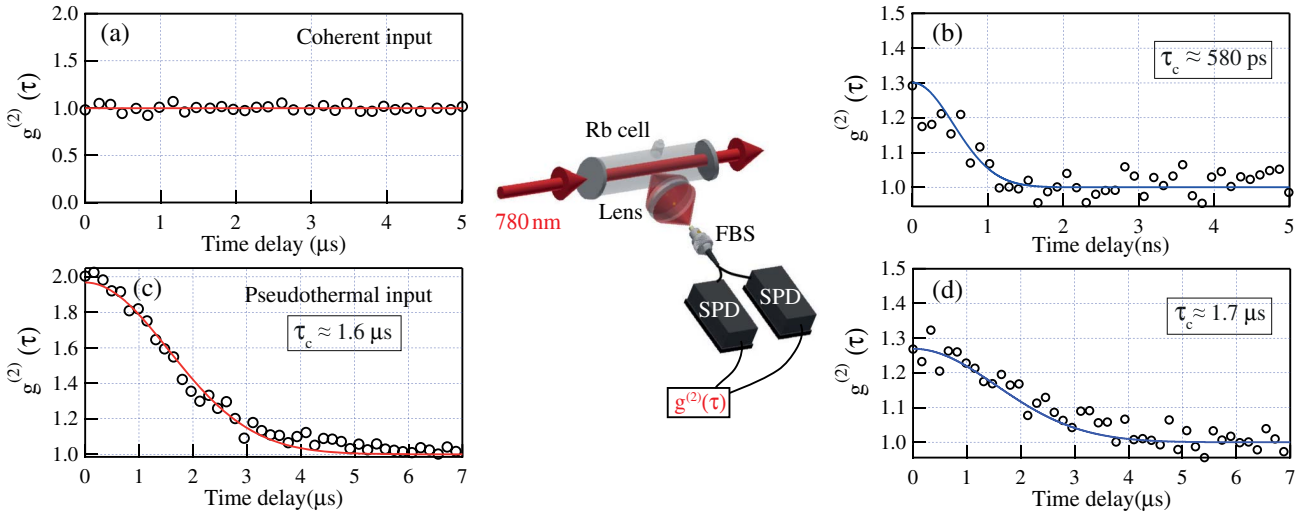

Fig. 4. $g^{(2)}(\tau)$ function obtained from the spontaneous emission of Rb vapor due to the 780 nm input beam with different photon statistics (correlated and uncorrelated intensity fluctuation). The figure at the center shows the experimental setup. (a) Coherent 780 nm input beam. (b) The $g^{(2)}(\tau)$ function of spontaneously emitted photons for the coherent 780 nm input. The measured coherence time becomes much shorter than the lifetime, 26 ns, of the excited $5P_{3/2}$ state due to Doppler broadening. The blue solid line is the theoretical curve described in Section 4. (c) Pseudothermal 780 nm input beam. The red-solid line represents a fitting result according to Eq. (2). (d) The $g^{(2)}(\tau)$ function of spontaneously emitted photons for the pseudothermal 780 nm input. Due to Doppler broadening, the photon bunching effect is significantly reduced compared to the input thermal beam. The blue solid line is the theoretical curve described in Section 4.

$\sigma[\omega'(1-\frac{v_x}{c})]$ with its full width at half-maximum given by $\Gamma = 2\pi \times 6.066$ MHz for the D_2 line of Rb; see Eq. (4). The first term in the second line represents the Maxwell–Boltzmann velocity distribution along the two directions and $u = \sqrt{\frac{2k_BT}{m}}$ is the mean velocity, where k_B is the Boltzmann constant, T is the temperature, and m is the atomic mass of ^{85}Rb. The Dirac delta function expresses energy conservation during the scattering process in the atomic rest frame.

Now, let us consider the Doppler broadening effect to atomic transition; see Fig. 5. This effect leads the incident laser to excite the Rb atom from the ground state $F = 3$ to all the excited levels allowed by the selection rules, and atoms then decay into the $F = 3$ and $F = 2$, which is due to the Raman scattering in the hyperfine ground states. The scattering cross section can then be modified by [22]

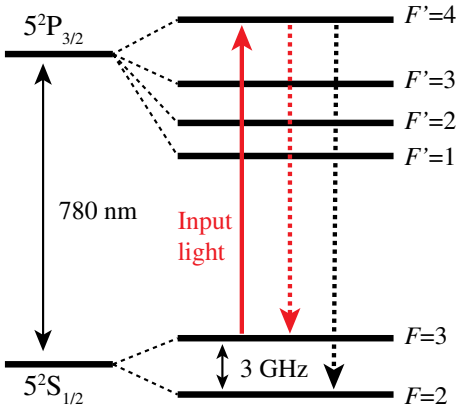

Fig. 5. Hyperfine structure of ^{85}Rb D_2 line. The black dotted line represents the emission through the Raman scattering.

$$\sigma(\omega_{\text{atom}}) = \sigma_0 \sum_{F=2}^{3}\sum_{F'=1}^{4} \frac{(2F+1)S_{FF'}}{1+4[\frac{\omega_{\text{atom}}-\omega_{FF'}}{\Gamma}]^2}, \tag{4}$$

where $\omega_{\text{atom}} = \omega'(1 - v_x/c)$. $S_{FF'}$ is the hyperfine transition strength factor [24] and $\omega_{FF'}$ is the transition frequency between the hyperfine ground state F and the excited state F'. Therefore, the emission spectrum reflecting multilevel transition and the Raman scattering due to the Doppler broadening can be expressed as [22]

$$\begin{aligned} S(\omega) \propto \int d\omega' dv_x dv_y S_0(\omega') \sum_{F_1=2}^{3}\sum_{F_2=2}^{3}\sum_{F'=1}^{4} e^{-\frac{v_x^2+v_y^2}{u^2}} \\ \times \frac{(2F_1+1)S_{F_1F'}}{1+4\left[\frac{\omega'(1-v_x/c)-\omega_{F_1F'}}{\Gamma}\right]^2} \frac{S_{F_2F'}}{\sum_{F=2}^{3} S_{FF'}} \\ \times \delta\left[\omega - \omega'\left(1-\frac{v_x}{c}\right)\left(1+\frac{v_y}{c}\right) - \omega_{F_1F_2}\right], \end{aligned} \tag{5}$$

where $\omega_{F_1F_2} \approx 2\pi \times 3$ GHz is the hyperfine splitting between the two ground states $F = 2$ and $F = 3$. F_1 and F_2 represent the initial and final states of the scattering process.

From the emission spectrum, we have calculated the second-order correlation function expressed by

$$g_{sp}^{(2)}(\tau) = 1 + |g_{sp}^{(1)}(\tau)|^2, \tag{6}$$

where

$$g_{sp}^{(1)}(\tau) = \frac{1}{2\pi}\int d\omega S(\omega) e^{-i\omega\tau}. \tag{7}$$

The calculated $g_{sp}^{(2)}(\tau)$ for the spontaneous emission under our experimental condition is shown in the inset of Fig. 6(a). For the coherent input light, the multilevel excitation and Raman

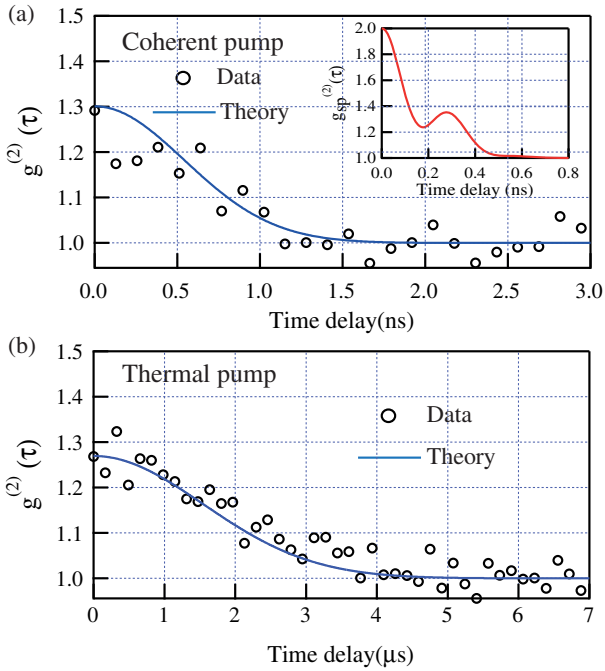

Fig. 6. Measured and theoretical $g^{(2)}(\tau)$ for the spontaneous emission. (a) For the coherent pump shown in Fig. 4(a). (b) For the thermal pump shown in Fig. 4(c). The inset in (a) shows $g^{(2)}_{sp}(\tau)$ obtained from the Fourier transform of $S(\omega)$. In (a), the blue solid line is the theoretical curve calculated from the convolution between the spontaneous emission and the timing resolution function. In (b), the solid line is the result of convolution between the thermal input $g^{(2)}(\tau)$ shown in Fig. 4(c) and the theoretical $g^{(2)}(\tau)$ curve from Fig. 6(a). The experimental data, from Figs. 4(b) and 4(d), are in agreement with the theoretical calculations.

scattering due to the Doppler broadening make the coherence time comparable to the timing resolution of the measurement electronics, which is much shorter than the excited-state lifetime of 26 ns. The timing resolution function $R(\tau)$ is experimentally measured to be a Gaussian function with the width of 500 ps. To account for the timing resolution of the measurement electronics to the measured second-order correlation function $g^{(2)}(\tau) = 1 + |g^{(1)}(\tau)|^2$, the convolution between $g^{(1)}_{sp}(\tau)$ and the timing resolution function $R(\tau)$ is calculated as follows [19,20]:

$$|g^{(1)}(\tau)| = |g^{(1)}_{sp}(\tau)| \star |R(\tau)|, \tag{8}$$

where $\star$ represents convolution integral.

Figure 6 shows the calculated and measured second-order correlation function for the spontaneous emission due to coherent and thermal pump conditions considered in Fig. 4. For the coherent pumping condition shown in Fig. 4(a), Fig. 6(a) shows the measured and calculated $g^{(2)}(\tau)$. It is clear that, when the timing resolution of the measurement electronics is considered, the measured data are in good agreement with the calculated $g^{(2)}(\tau)$. For the thermal pumping condition shown in Fig. 4(c), the calculated and measured $g^{(2)}(\tau)$ are shown in Fig. 6(b). For calculating $g^{(2)}(\tau)$ in this case, we use the relation $g^{(2)}(\tau) = 1 + |g^{(1)}(\tau)|^2$ for thermal light. By calculating the convolution between the Doppler broadened $g^{(1)}(\tau)$ and the pseudothermal input $g^{(1)}(\tau)$, we obtain the $g^{(2)}(\tau)$ function for the thermal pumping condition. The reduction of $g^{(2)}(0)$ due to the Doppler broadening effect is clearly shown in Fig. 6(b). For the thermal input light with the coherence time of a few microseconds, the coherence time of the spontaneous emission does not change significantly, since the input thermal light has the coherence time much bigger than that of the Doppler broadening. The limited timing resolution mainly contributes to reducing the peak value of $g^{(2)}(0)$. The photon bandwidth due to the spontaneous emission therefore cannot be separated from the characteristics of the input field and thus affect the $g^{(2)}(0)$ value. This result indirectly confirms that the reduced $g^{(2)}(0)$ of the 420 nm CBL beam is caused by the Doppler broadening in the Rb vapor.

5. CONCLUSION

We have experimentally demonstrated intensity correlation transfer of input fields in the CBL generation process in ^{85}Rb atomic vapor. By preparing the input beams at 780 nm and 776 nm into thermal light, hence Bose–Einstein statistics, we test whether the 420 nm CBL beam generated via the parametric FWM process retains the intensity correlation of the input beam. The $g^{(2)}(\tau)$ intensity correlation measurement of the CBL field reveals that the intensity correlation properties of the input fields are transferred to the CBL field due to strong atomic coherence in the FWM loop. While the 420 nm CBL beam does show bunching, the net effect is less than the ideal value of $g^{(2)}(0) = 2$. This result has been investigated theoretically, and the theoretical results clearly show that the reduced $g^{(2)}(0)$ values in the HBT measurement result from Doppler broadening in the Rb vapor.

Funding. National Research Foundation of Korea (NRF) (2016R1A2A1A05005202, 2016R1A4A1008978, 2015H1A2A1033028).

Acknowledgment. We thank Y.-C. Jeong, T. Zhao, Y.-W. Cho and H. S. Moon for helpful comments. Y. K. acknowledges the Global Ph.D. Fellowship by the National Research Foundation of Korea.

REFERENCES

1. A. S. Zibrov, M. D. Lukin, L. Hollberg, and M. O. Scully, "Efficient frequency up-conversion in resonant coherent media," Phys. Rev. A **65**, 051801 (2002).
2. T. Meijer, J. D. White, B. Smeets, M. Jeppesen, and R. E. Scholten, "Blue five-level frequency-upconversion system in rubidium," Opt. Lett. **31**, 1002–1004 (2006).
3. F. E. Becerra, R. T. Willis, S. L. Rolston, and L. A. Orozco, "Nondegenerate four-wave mixing in rubidium vapor: the diamond configuration," Phys. Rev. A **78**, 013834 (2008).
4. J. T. Schultz, S. Abend, D. Doring, J. E. Debs, P. A. Altin, J. D. White, N. P. Robins, and J. D. Close, "Coherent 455 nm beam production in a cesium vapor," Opt. Lett. **34**, 2321–2323 (2009).
5. A. Akulshin, R. McLean, A. Sidorov, and P. Hannaford, "Coherent and collimated blue light generated by four-wave mixing in Rb vapour," Opt. Express **17**, 22861–22870 (2009).
6. A. Vernier, S. Franke-Arnold, E. Riss, and A. S. Arnold, "Enhanced frequency up-conversion in Rb vapor," Opt. Express **18**, 17020–17026 (2010).

7. J. F. Sell, M. A. Gearba, B. D. DePaola, and R. J. Knize, "Collimated blue and infrared beams generated by two-photon excitation in Rb vapor," Opt. Lett. **39**, 528–531 (2014).
8. G. Walker, A. S. Arnold, and S. Franke-Arnold, "Trans-spectral orbital angular momentum transfer via four-wave mixing in Rb vapor," Phys. Rev. Lett. **108**, 243601 (2012).
9. A. Akulshin, R. McLean, E. Mikhailov, and I. Novikova, "Distinguishing nonlinear processes in atomic media via orbital angular momentum transfer," Opt. Lett. **40**, 1109–1112 (2015).
10. A. Akulshin, I. Novikova, R. McLean, E. Mikhailov, S. Suslov, and R. McLean, "Arithmetic with optical topological charges in stepwise-excited Rb vapor," Opt. Lett. **41**, 1146–1149 (2016).
11. Y. W. Cho and Y.-H. Kim, "Storage and retrieval of thermal light in warm atomic vapor," Phys. Rev. A **82**, 033830 (2010).
12. I.-H. Bae, Y.-W. Cho, H. J. Lee, Y.-H. Kim, and H. S. Moon, "Superluminal propagation of pulsed pseudo-thermal light in atomic vapor," Opt. Express **18**, 19693–19699 (2010).
13. Y.-W. Cho, J.-E. Oh, and Y.-H. Kim, "Storage and retrieval of ghost images in hot atomic vapor," Opt. Express **20**, 5809–5816 (2012).
14. Y.-W. Cho, J.-E. Oh, and Y.-H. Kim, "Diffusion-free image storage in hot atomic vapor," Phys. Rev. A **86**, 013844 (2012).
15. O. S. Heavens, "Radiative transition probabilities of the lower excited states of the alkali metals," J. Opt. Soc. Am. **51**, 1058–1061 (1961).
16. R. Hanbury-Brown and R. Q. Twiss, "Correlation between photons in two coherent beams of light," Nature **177**, 27–29 (1956).
17. F. T. Arecchi, "Measurement of the statistical distribution of Gaussian and laser sources," Phys. Rev. Lett. **15**, 912–916 (1965).
18. R. Loudon, *The Quantum Theory of Light* (Oxford University, 2000).
19. S. Bali, D. Hoffmann, J. Siman, and T. Walker, "Measurement of intensity correlation of scattered light from laser-cooled atoms," Phys. Rev. A **53**, 3469–3472 (1996).
20. A. Dussaux, T. Passerat de Silans, W. Guerin, O. Alibart, S. Tanzilli, F. Vakili, and R. Kaiser, "Temporal intensity correlation of light scattered by a hot atomic vapor," Phys. Rev. A **93**, 043826 (2016).
21. Y.-W. Cho, H.-T. Lim, Y.-S. Ra, and Y.-H. Kim, "Weak value measurement with an incoherent measuring device," New J. Phys. **12**, 023036 (2010).
22. N. Mercadier, M. Chevrollier, W. Guerin, and R. Kaiser, "Microscopic characterization of Levy flight of light in atomic vapor," Phys. Rev. A **87**, 063837 (2013).
23. A. Zhang, Y. Zhai, and L. Wu, "Correlated two-photon imaging with true thermal light," Opt. Lett. **30**, 2354–2356 (2005).
24. D. A. Steck, Rubidium 87 D line data (2008), http://users.df.uba.ar/schmiegelow/materias/labo5_2017v/rubidium85numbers.pdf.